Study of the Glass Transition Temperatures of Stereoregular PMMAs Using Different Force Fields

Armand Soldera,* Noureddine Metatla

Département de Chimie, Université de Sherbrooke, Sherbrooke, J1K 2R1, Canada

Internet Electronic Conference of Molecular Design **2003**, November 23 – December 6

Abstract

Motivation. To describe the glass transition phenomenon using molecular modeling, poly(methyl methacrylate), PMMA, offers a noteworthy regard since according to the tacticity of its chain, a different T_g is displayed. Accordingly, if a force field accurately describes such variation, insights can be gained in the understanding of the reasons that give rise to this difference, and consequently, in the glass transition phenomenon itself. Several studies have been carried out using a second category force field, *pcff*. In this article, two first class force fields, AMBER and AMBER/OPLS, have been envisioned. It is found that, although T_gs are obtained at higher temperatures, the difference between the two T_gs is better mimicked using the AMBER/OPLS force field. The presence of the cross terms in the force fields is thus not a determining factor in obtaining the T_gs variation.

Method. Molecular dynamics simulations have been employed to compare glass transition of stereoregular polymers, and their energetic differences, with respect to the use of two force fields of different generation..

Results. A first generation force field could deal with the representation of the difference in T_gs between stereoregular polymers.

Conclusions. Accordingly to the fact that a first generation force field can deal with the difference in T_gs difference, a greater amount of phase space could be regarded. Moreover, studies of specific interaction, such as PMMA behavior with surfaces, can be undertaken.

Availability.

Keywords. Glass transition temperature, steroregular PMMA, AMBER/OPLS, molecular dynamics

Abbreviations and notations

Collect here in alphabetical order all abbreviations and	notations used in the paper
MD, molecular dynamics	PMMA, poly(methyl metha crylate)
i-PMMA, isotactic PMMA	s-PMMAi, syndiotactic PMMA

1 INTRODUCTION

Molecular modeling of polymers is becoming more and more relevant for industrial applications and academia researches. Such an increase stems from different factors: increase of computer efficiency, availability of commercial codes with attractive environment, and improvement of force fields. The choice of a force field could have dramatic effect on the value of the final properties. Nevertheless with present second category force field such as COMPASS [1], MM4 [2], the probability that an atom is not correctly documented has considerably decreased. Actually such a high transferability is not always requested. The use of a first category force field where no cross-terms are present, has several advantages: each energetical term in the force field mathematical formulation possesses its proper physical significance, less CPU (Central Process Unit) time is requested. In an SGI Octane 2000, for the same system with all internal and external conditions equivalent (duration, integration time, thermostat, barostat, …), the requested CPU time using a first category force field is reduced by a factor of 4 comparatively to the use of the second

* Correspondence author; phone: +1-819-821-7650; fax: +1-819-821-7650; E-mail: Armand.Soldera@Usherbrooke.ca

category force field, *pcff*. Moreover, it has to be pointed out that the physical significance of the cross-terms inside a second category force field is still a source of debate [3]. In the perspective to better understanding specific differences observed between stereoregular PMMAs, the physical significance of each mathematical form inside a force field is a relevant parameter. Moreover using a first generation force field a greater phase space could be regarded with a less amount of CPU time. Finally, a better description from a phenomenological or theoretical viewpoint can be addressed to the property of interest.

Poly(methyl methacrylate), PMMA, whose repeat unit is displayed in Fig. 1, is actually an ideal polymer to study physical properties using molecular modeling. According to the tacticity of its chain, different experimental properties are exhibited: solubilities, crystal structures [4], …

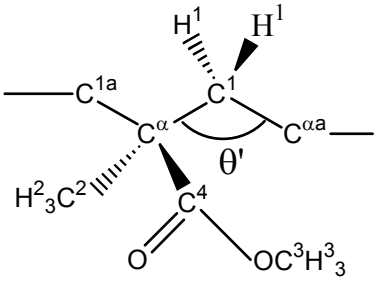

Figure 1. PMMA repeat unit.

Accordingly, these variations in the properties can be interpreted in changes in molecular characteristics only. As a matter of fact, if a force field can appropriately deal with these differences, further analyses on the reasons that give rise to these variations can be undertaken. Consequently insights of the tricky problem of the difference in the glass transition temperatures between the two PMMA configurations, and thus in the glass transition itself, can be revealed. Several studies have been carried out using the second category force field, *pcff* [5, [6, [7, [8]; however, the glass transition difference has not yet been observed using a first category force field. In fact, several studies on PMMA have been concerned by the use of a first class force field [9, [10], but the difference in properties of the two PMMA configurations has only been addressed by the AMBER force field. The computed property was the solubility parameter. This article is thus concerned by the study of the influence of the employed force field to deal with the difference in the T_gs between the two PMMA configurations. A particular attention will be paid on the selection of the first generation force field to accurately display the difference in the T_gs between the two configurations. Results on the difference in "static" properties are presented. A subsequent paper will expose the dynamics conclusions.

2 SIMULATION METHODS

2.1 Force field

A polymer contains a great number of atoms. Consequently, empirical methods, that are molecular mechanics and dynamics, are currently used to deal with polymer simulation. Both methods are based on the use of a force field. Accordingly, the quality of the employed force field for the simulation will have a major impact on the final results. It actually depends on different factors. A force field expresses the average electronic interaction between atoms [11]. Different terms are thus included in its formulation to mimic all the forces that exist between the atoms. Specific equations are then used to fit such interaction. However, these equations could differ from the degree of their Taylor expansion, or from their functional form. For instance, the covalent bond can be depicted by a Morse function, a Hooke's law, a quartic equation, or a higher Taylor expansion of the Morse function (MM4) [2]. These fittings thus generate an ensemble of parameters for an atom in a specific environment, usually called potential. It has to be noted that the parameterization depends on many aspects [12]: data used for the fitting (experimental data or first principle calculations), mathematical expression, etc... The large amount of electronic environments of an atom yields to numerous potentials for this atom. In fact, the number of these potentials for an atom greatly differs among force fields. A high transferability force field possesses numerous potentials for one atom; for instance the carbon atom possesses 20 different potentials in the *pcff* force field [13]. Actually the mathematical expression and the atomic potentials defines a "force field" [14]. Consequently, the building of a force field request particular attention. The present study is thus limited to the use of existing force field since the goal is to find a first class force field that is enabled to accurately mimic the difference in interactions between the two PMMA configurations.

The force field equation is usually divided into two major groups: the intramolecular terms that take into account the connectivity and the flexibility of the polymer chains, and the intermolecular functions, or non-bond terms, that are constituted by a repulsive, a dispersive and an electrostatic terms. A classification is usually made among force fields by considering the presence or not of cross-terms in the intramolecular part: they actually appear only in the second category force field [3]. These cross-terms are also referred as off-diagonal terms since they tend to express the influence of one internal parameter to an adjacent one.

In this paper the two generations of force fields are compared regarding to the difference in displaying the simulated glass transition. An exhaustive study of the difference between the two generation force fields is under the scope of this article. As already outlined, the aim is to get a first generation force field that accurately expresses the difference in T_gs between the two PMMA configurations. Accordingly, such force field will be used for subsequent analyses.

The second category force field used to simulate the glass transition phenomenon is *pcff* [13]. This force field has especially built up to work with a great variety of polymers. Two first category force fields have been used. They actually derived from the AMBER force field [15]. The reason to select AMBER comes from the fact that it was used to study the difference in the solubility parameters between the two PMMA configurations [4]. It has to be mentioned that the first class force fields DREIDING, was employed to simulate PMMA; the isotactic configuration [16] and the syndiotactic configuration [10], have been simulated separately. The other force field that has been used for this study, AMBER/OPLS, differ from the original AMBER force field, by the way the partial charges have been obtained.

The mathematical expressions of *pcff* and the first generation force fields are presented in Eq. 1 and 2, repectively.

$$
\begin{aligned}
V = & \sum_{b}\left[K_2\left(b-b_0\right)^2+K_3\left(b-b_0\right)^3+K_4\left(b-b_0\right)^4\right]+\sum_{\theta}\left[H_2\left(\theta-\theta_0\right)^2+H_3\left(\theta-\theta_0\right)^3+H_4\left(\theta-\theta_0\right)^4\right] \\
& +\sum_{\phi}\left[V_1\left[1-\cos\left(\phi-\phi_1^0\right)\right]+V_2\left[1-\cos\left(2\phi-\phi_2^0\right)\right]+V_3\left[1-\cos\left(3\phi-\phi_3^0\right)\right]\right]+\sum_{\chi}K_\chi\chi^2 \\
& +\sum_{b}\sum_{b'}F_{bb'}\left(b-b_0\right)\left(b'-b'_0\right)+\sum_{\theta}\sum_{\theta'}F_{\theta\theta'}\left(\theta-\theta_0\right)\left(\theta'-\theta'_0\right)+\sum_{b}\sum_{\theta}F_{b\theta}\left(b-b_0\right)\left(\theta-\theta_0\right) \\
& +\sum_{b}\sum_{\phi}\left(b-b_0\right)\left[V_1\cos\phi+V_2\cos 2\phi+V_3\cos 3\phi\right]+\sum_{b'}\sum_{\phi}\left(b'-b'_0\right)\left[V_1\cos\phi+V_2\cos 2\phi+V_3\cos 3\phi\right] \\
& +\sum_{\theta}\sum_{\phi}\left(\theta-\theta_0\right)\left[V_1\cos\phi+V_2\cos 2\phi+V_3\cos 3\phi\right]+\sum_{\phi}\sum_{\theta}\sum_{\theta'}K_{\phi\theta\theta'}\cos\phi\left(\theta-\theta_0\right)\left(\theta'-\theta'_0\right) \\
& +\sum_{i>j}\frac{q_iq_j}{\varepsilon r_{ij}}+\sum_{i>j}\varepsilon_{ij}\left[2\left(\frac{r_{ij}^*}{r_{ij}}\right)^9-3\left(\frac{r_{ij}^*}{r_{ij}}\right)^6\right]
\end{aligned}
\tag{1}
$$

K_2, K_3, K_4, H_2, H_3, H_4, V_1, V_2, V_3, b_0, θ_0, ϕ_1^0, ϕ_2^0, ϕ_3^0, ε_{ij}, r^*_{ij}, q_i, q_j, are potential parameters included into the force field. b, θ, ϕ, r_{ij}, are bond length, valence angle, dihedral angle, and non-bonding distance between two atoms i and j, respectively. These parameters are got during simulation, and allow the computation of the energetical values that will be reported in this article.

$$
\begin{aligned}
V = & \sum_{b}K\left(b-b_0\right)^2+\sum_{\theta}H\left(\theta-\theta_0\right)^2 \\
& +\sum_{\phi}\left[V_1\left[1-\cos\left(\phi-\phi_1^0\right)\right]+V_2\left[1-\cos\left(2\phi-\phi_2^0\right)\right]+V_3\left[1-\cos\left(3\phi-\phi_3^0\right)\right]\right] \\
& +\sum_{i>j}\frac{q_iq_j}{\varepsilon r_{ij}}+\sum_{i>j}4\varepsilon_{ij}\left[\left(\frac{\sigma_{ij}}{r_{ij}}\right)^{12}-\left(\frac{\sigma_{ij}}{r_{ij}}\right)^6\right]
\end{aligned}
\tag{2}
$$

K, H, V_1, V_2, V_3, b_0, θ_0, ϕ_1^0, ϕ_2^0, ϕ_3^0, ε_{ij}, σ_{ij}, q_i, q_j, are potential parameters included into the force field. b, θ, ϕ, r_{ij}, are bond length, valence angle, dihedral angle, and non-bonding distance between two atoms i and j, respectively. These parameters are got during simulation.

The different fitting parameters, except for cross-terms, used for the simulations are presented in Appendix 1 for the non-bonding term, Appendix 2 for the partial charges of the electrostatic term, Appendix 3 for the bonding term, Appendix 4 for the valence angle term, and Appendix 5 for the

torsion term. The AMBER type convention for potentials is employed: CT = sp^3 carbon, C = carbonyl carbon, HC = hydrogen attached to carbon, O = carbonyl oxygen, OS = ethyl and ester oxygen.

A special remark has to be made concerning the non-bond parameters, more precisely the partial charges. Two sets have been used for the first category force field. The first set directly stems from the AMBER force field that have been used to compute the solubility parameters of the two PMMA configurations [4]. These charges have been computed from the crystal structure of PMMA. Actually they could vary according to their environment. This article is only concerned by the influence of static charges. Nevertheless comments on the final results will be discussed on the utility of varying charges or not in our specific studies. The second set corresponds to the OPLS partial charges [17]. The OPLS charges have been determined to fit experimental density and vaporization enthalpies. They actually show a great success to model liquids.

2.2 Computer Software

An important step in the molecular modeling of polymers is the accurate depiction of the phase space. Since the ergodic hypothesis is never fulfilled, a specific procedure has to be carried out to give the best representation of the configurational space. The choice of the configurations that will be embedded in a cell using the periodic boundary conditions [18], is crucial. One polymer chain with one hundred repeat units (RU), actually propagate into the periodic box according to the self-avoiding walk [19] technique with the long-range non-bonded interactions described by Theodorou and Suter [20]. The procedure is implemented in the Accelrys *Amorphous_Cell*© software. The selection of the configurations that will be used during simulation, follows a specific procedure. Thirty configurations have been initially generated using the *pcff* force field. Comparing the end-to-end distance of each configuration and the predicted one, using the RIS model, makes a first selection. The second choice was made from an energetic viewpoint: after a relaxation procedure (molecular dynamics and minimization), the configurations with the highest energy are rejected. Finally ten configurations for each polymer configurations have been selected for the simulation of the glass transition. The values of the end-to-end distances are presented in Appendix 1. 51 ± 10 Å, and 33 ± 10 Å, for i-PMMA, and s-PMMA, respectively. The higher value of the end-to-end distance for i-PMMA is in agreement with expected values [21].

The DL_POLY code was then used for each polymer conformation [22]. The integration of the Newtonian equations of motion to carry out the MD simulation using the two force fields have been done through the same pattern: the leap-frog variant of the velocity Verlet algorithm with an integration step of 0.001 ps, and a duration of 100 ps. During MD simulations with the *pcff* force field, the pressure was controlled according to the Parrinello-Rahman algorithm [23], while the temperature was imposed, in the primary step by the velocity-scaling algorithm, and then through the Andersen algorithm [24]. The Berendsen thermostat and barostat were used to keep the system

at prescribed temperatures and pressures [25]. The non-bonded interactions have been computed using the Ewald summation; a non-bond cut-off of 10 Å was selected.

2.3 Dilatometric Simulation

To get the T_g, the simulated dilatometry technique has been employed [26]. As in the experimental dilatometry technique, the specific volume, i.e. the inverse of the density, is reported with respect to the temperature (Figs 2 and 3). The intercept of the lines joining the points of the two phases, the vitreous and rubbery, yields the value of the T_g. In order to acquire the density at a desired temperature, molecular dynamics, MD, simulations were performed in the NPT statistical ensemble, i.e. constant number of particles, pressure and temperature. The simulated density directly stems from the knowledge of the periodic box volume.

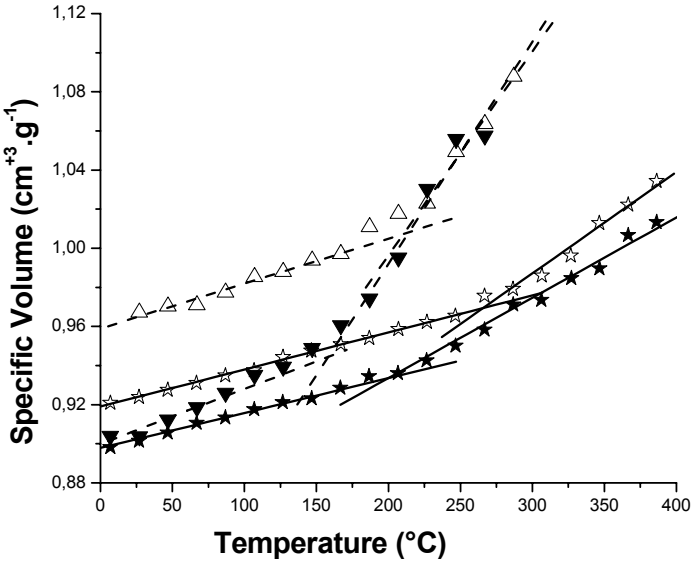

Figure 2. Simulated dilatometric curves for the two PMMA configurations according two force fields: i-PMMA (◆), and s-PMMA (□) through the *pcff* force field simulation, and i-PMMA (□), and s-PMMA (□) through the AMBER force field simulation.

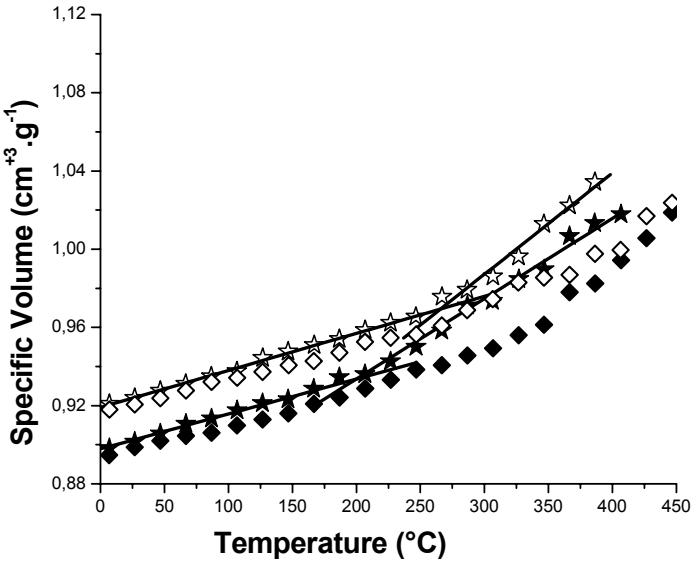

Figure 3. Simulated dilatometric curves for the two PMMA configurations according two first category force fields: i-PMMA (▼), and s-PMMA (△) through the AMBER force field simulation, and i-PMMA (□), and s-PMMA (□) through the AMBER/OPLS force field simulation.

3 RESULTS AND DISCUSSION

3.1 Simulated Dilatometric Results

Comparison between simulated dilatometric graphs obtained for the two PMMA configurations using the different force fields are displayed in Figs 2 and 3. It has to be pointed out, that with a view to clarity, standard deviations are not displayed (in order of 0.005 g.cm^{-3} below T_g and 0.01 g.cm^{-3} above T_g), and dilatometric curves are not shown in the same graph. Nevertheless, the curves are arranged by pair, and the data with the AMBER/OPLS force field are the reference. Those data are thus compared to AMBER, and *pcff* results in Fig. 2, and 3, respectively. The values of the T_gs for both PMMA configurations and their difference are compared to experimental data in Table 1.

Table 1. Experimental and simulated glass transition temperatures using the different force fields described in the text, for both PMMA configurations

Force field	T_g (i-PMMA) (°C)	T_g (s-PMMA) (°C)	ΔT_g
pcff	157	212	55
AMBER	322	338	16
AMBER/OPLS	201	265	64
Experimental	45	114	69

First conclusions can be extracted from data of Fig. 3 and Table 1. Using the AMBER force field, determination of the T_g for the two PMMA configurations is not rigorous. Actually, a great range of transition temperatures could be obtained. However, the T_gs obtained using simulation with the AMBER force field, are clearly higher than those with AMBER/OPLS force field. The only difference between the two force fields is the way the partial charges that are present in the coulombic term, are computed.

Using *pcff*, and AMBER/OPLS force fields, the difference in T_gs between the two PMMA configurations is clearly exhibited: it is found to be 54 °C for *pcff*, and 64 °C for AMBER/OPLS. These values have to be compared with the 69 °C experimentally obtained. It has to be pointed out that the experimental difference takes into account the mass of the polymer through the use of the Fox-Flory equation [5]. A possible explanation of the better representation of this difference by the AMBER/OPLS force field could stem from the better representation of the phase space. However, the absolute values of the T_gs using the AMBER force field are clearly found superior than the experimental ones. Such a difference could be explained from two viewpoints. Firstly, the quenching rate is in order of 10^9 times more rapid than an experimental quenching rate. According to the time-temperature superposition principle, the T_g has to be higher than the experimental one. Secondly, as mentioned by Boyd et al. the value of the dihedral potential has a great impact on the value of the T_g: higher is the dihedral potential higher is the T_g [27]. Such a behavior is in agreement with the value of the dihedral potentials of the two force fields, presented in Appendix 5. For instance, the AMBER force field exhibits a cross-barrier energy for a torsion along the backbone in order of 0.50 kcal.mol^{-1} higher than for the same torsion in the *pcff* force field. Accordingly, more thermal energy is necessary to cross the energetic barrier according to the free volume theory; and thus higher is the T_g.

The volumetric thermal coefficient, α, is also a parameter that can be directly obtained from dilatometric curves. It has to be pointed out that the volumetric thermal coefficients are comparable for the two first category force fields used in this present study. As a matter of fact, only the simulated volumetric thermal coefficients using the AMBER/OPLS and *pcff* force fields, are compared to experimental ones in Table 2 [5]. In the vitreous state, the α coefficient is slightly underestimated in the case of simulation using the AMBER/OPLS force field. In the rubbery state, it is also slightly below the experimental value, but in the case of the *pcff* force field, the coefficient is two times the experimental value. As suggested by Fan et al., the increase of uncertainties could be responsible for the discrepancy of the α value noticed at temperatures above T_g [28]. Another explanation stays in the poor representation of the phase space. In fact, once the configurational space has been selected, all the MD trajectories at different temperatures are restrained around these points in the phase space. In the rubbery phase, a greater amount of the phase space has to be explored: the variation in entropy drastically increases. Since more configurations are used, better is the phase space representation, and better is thus the value of α. Finally, the difference in the

specific volume between the two PMMA configurations obtained using the AMBER/OPLS force field, 0.02 $cm^3.g^{-1}$ is in the same order than the experimental one, 0.018 $cm^3.g^{-1}$ [29].

Table 2. Experimental volumetric thermal expansion coefficients, α, and by simulations using the AMBER/OPLS and *pcff* force fields, for both PMMA configurations, in the vitreous and rubbery phases.

State	Configuration	Experimental	pcff	AMBER/OPLS
vitreous	i-PMMA	$2.7\ 10^{-4}\ K^{-1}$	$3.0\ 10^{-4}\ K^{-1}$	$2.0\ 10^{-4}\ K^{-1}$
	at-PMMA			
	s-PMMA		$2.4\ 10^{-4}\ K^{-1}$	$2.0\ 10^{-4}\ K^{-1}$
rubbery	i-PMMA	$5.7\ 10^{-4}\ K^{-1}$	$11.0\ 10^{-4}\ K^{-1}$	$4.2\ 10^{-4}\ K^{-1}$
	at-PMMA			
	s-PMMA		$10.0\ 10^{-4}\ K^{-1}$	$5.2\ 10^{-4}\ K^{-1}$

Molecular modeling can deal with the difference in the glass transition temperatures between the two PMMA configurations for both category force fields. Nevertheless in the case of the first category force field, the effective charges that derive from experimental data obtained with liquids show a better representation of the glass transition than those extracting from computational methods. Since QEq charges are computed from the PMMA crystal structure, they are not adapted to simulate "liquid" like behavior. Since OPLS charges yield to accurate results, variations of QEq charge values have not been undertaken. Moreover, such calculations request more CPU time. As a matter of fact, and since the values of the T_gs have not been accurately documented, data extracted from the simulations using the AMBER force field with QEq charges, will not be envisioned. Energy and internal parameters are thus extracted from simulations using the *pcff* and AMBER/OPLS force fields. Their values have been determined from the averages performed on the MD trajectories of the 10 selected configurations, and compared to published results obtained from simulation using the *pcff* force field. Such procedure has published elsewhere.

3.2 Properties

3.2.1. Energetical properties

A complete energetical description of the two PMMA configurations for simulations using the *pcff* force field has been already described [6]. The attention is thus focused on the differentiation between results extracted from the simulations using the two category force fields.

Non-bond energy

The intermolecular energy of the syndiotactic chain is found higher than in the case of the isotactic chain for both category force fields: the difference is 20 $kcal.mol^{-1}$ in the case of the AMBER/OPLS force field, and 35 $kcal.mol^{-1}$ in the case of the *pcff* force field [6]. The higher value for s-PMMA explains its lower density comparatively to the i-PMMA chain (Fig. 3). Such a behavior agrees with the free volume theory to explain the difference in the T_gs. Higher is the non-

bond energy, lower is the ability of the chain to crossover the energetic barrier, and thus to move more easily, and thus higher is the T_g. However, this difference could not explain the important difference of T_gs between the two PMMA configurations. Moreover, the greater difference in the non-bond energy found in *pcff* simulation compared with AMBER/OPLS simulation is not in accordance with the observed lower difference in the T_gs (Fig. 3). Further energetical analyses have thus to be pursued.

Intramolecular energy

Simulations using the two force field exhibit a difference in the intramolecular energy between the two PMMA configurations: 45, and 72 kcal mol^{-1}, for *pcff* and AMBER/OPLS force fields, respectively. For both kind of simulation, the dominant difference in intramolecular energy terms comes from the valence angle term [6]. The two other non-cross terms, the bonding and dihedral energy functions, do not exhibit significant differences; they are actually included in the standard mean deviation. The variation in the valence energy between the two PMMA configurations is different: 75, and 35 kcal mol^{-1} for *pcff*, and AMBER/OPLS force fields, respectively.

To determine the angle responsible for this difference, all the valence angles have been regarded; the procedure has been published elsewhere. A slight difference exists between results stemming from the two force fields. In Table 3 are presented only the backbone angles extracting from the different simulations; they actually contribute the most to the difference in energy. The major contribution stems from the difference in the intra-diade angle. This aperture is actually due to lessen the side-chain interactions [21]. Since such interactions are different according to the tacticity of the PMMA chain, antiferro or ferro-like, the aperture is found less important for s-PMMA than for i-PMMA. This variation is observed in both cases but with different values: 1.1 deg. and 0.6 deg. of difference for *pcff* and AMBER/OPLS respectively. This difference has to be compared to the difference in the valence energy, reported above. From Appendix 4, it is seen that for a CT-CT-CT (CT corresponds to an sp3 atom in the AMBER notation of atomic potentials) angle, the equilibrium value is different: 112.67° in the case of *pcff*, and 109.5° for AMBER/OPLS. Consequently, to compensate the same amount of energy, the intradiade angle aperture is less pronounced using the AMBER/OPLS force field. Such results have to be correlated to previous results on non-bond energy.

Table 3. Comparison of the backbone angles between the force fields described in the text, for both PMMA configurations

Angle	Configuration	PCFF	AMBER/OPLS
Intra-diade (τ)	i-PMMA	127.8 ± 0.1	128.7 ± 0.05
	s-PMMA	126.6 ± 0.1	128.1 ± 0.1
Inter-diade (τ')	i-PMMA	106.7 ± 0.2	108.7 ± 0.4
	s-PMMA	106.6 ± 0.2	108.3 ± 0.2

Simulations using the *pcff* force field exhibit higher non-bond valence energy differences than simulations with the AMBER/OPLS force field. Such results seem not to agree with the fact that simulation with *pcff* exhibits the lower difference in T_gs: according to the free volume theory, higher is the non-bond energy, higher is the T_g, and greater is the backbone angle aperture, higher is the mobility of the chain, and thus lower is the T_g. Consequently, simulation using the *pcff* force field would exhibit the greater difference. To explain the reason of such a difference in the results between the two force fields, the absolute values of the T_gs have to be regarded. In the case of the AMBER/OPLS force field, the T_gs are the highest. At such temperature range, the kinetic energy brought to the system is important. Accordingly, the general motion of atoms increases, and the mobility thus enhances. Therefore, to explain the difference in T_gs, the mobility of the two chains has to be different. Consequently, by a glimpse of the energetical parameter differences, and by looking at the variations between the results brought by simulations using the two force field results, insight of the difference in T_gs between the two configurations could be gained. Actually, local dynamics analysis confirm this finding.

Dilatometric and energetic results clearly show that the elimination of cross terms in the force fields does not greatly affect the interpretation of the difference in T_gs between the two PMMA configurations. One advantage of using a first category force field is that energetic representation is simplified. Accordingly, less parameters are needed for further simulations of PMMA involving the glass transition phenomenon. Moreover, a better depiction of the phase space is permitted with AMBER without requesting too much CPU time; and thus the entropic contribution is better represented and the quasi-ergodic hypothesis, although not satisfied, is better addressed. However, attention has to be particularly paid when dealing with a first category force field. In the case of the AMBER force field, it has been seen that the use of static QEq charges greatly affects the value of the T_g. This result could be explained by the fact that these charges have been computed one time for PMMA in its crystalline form. Moreover, the intramolecular terms could be modified. For instance the backbone angle parameters have been changed, and the CHARMM values have been chosen: in the case of CT-CT-CT, according to Appendix 4, h = 58.53 kcal mol^{-1} deg^{-2}, and θ_o =112.7 deg [30]. The equilibrium value is comparable to the 112.74 deg. of the *pcff* force field (Appendix 4). In this case, the difference in T_gs is reduced and the absolute values of the T_gs significantly increase. No real conclusion can be extracted from these changes since both equilibrium and stiffness constant have been changed. An exhaustive research of the best first category force field is under the scope of the present study. The important fact is to get an accurate representation of the glass transitions of stereoregular PMMAs, of a first category force field.

4 CONCLUSIONS

This article shows that the difference in the T_gs between the two PMMA configurations can be revealed by a first or second category force field. From an energetical analysis, simulation using

these two category force fields reveal comparable behavior: higher non-bond energy for the syndiotactic configuration, in agreement with the free volume theory, higher valence energy that is due to a greater aperture of the intra-diade angle for i-PMMA to lessen the interactions of the side-chains. Nevertheless, the difference in T_gs using the first category force field AMBER/OPLS is in better agreement with experimental data, than in the case of simulation using the second category force field *pcff*. Accordingly, further analyses that actually request a great portion of the phase space can be undertaken, using the AMBER/OPLS force field.

Acknowledgment

The work has been possible through the financial support of the Natural Sciences and Engineering Research Council of Canada and Université de Sherbrooke, the computer facilities of the Réseau Québécois de Calcul Haute Performance, the Canada Foundation for Innovation, and the Institut Supérieur des Matériaux et Mécaniques Avancés du Mans. The authors also wish to thank Pr. Y. Grohens for fruitful scientific discussion, and Pr. A.-M. Tremblay for the use of its computer cluster, Elix2.

Appendix 1

Parameters for non-bonding energetic term; a) for AMBER; b) for *pcff* force fields. For clarity, the mathematical expression is presented.

a) AMBER/OPLS $4\varepsilon_{ij}\left[\left(\frac{\sigma_{ij}}{r_{ij}}\right)^{12}-\left(\frac{\sigma_{ij}}{r_{ij}}\right)^{6}\right]$ with $\varepsilon_{ij}=\left(\varepsilon_i\varepsilon_j\right)^{1/2}$ and $\sigma_{ij}=\left(\sigma_i\sigma_j\right)^{1/2}$

atoms	σ_i (Å)	ε_i (kcal.mol^{-1})	Ref.
CT	3.500	0.066	1
C	3.750	0.105	2
OS	3.000	0.170	2
O	2.960	0.210	2
HC	2.500	0.030	1

1) W. L. Jorgensen et al*., J. Am. Chem. Soc*., **118**, 11225(1996); 2) M. L. P. Price et al., *J. Comp. Chem.*, **22**, 1340 (2001)

b) AMBER

$\left[\frac{A_{ij}}{R_{ij}^{12}}-\frac{B_{ij}}{R_{ij}^{6}}\right]$ with $R_{ij}^{*}=R_i^{*}+R_j^{*}$, $A_{ij}=\varepsilon_{ij}\left(R_{ij}^{*}\right)^{12}$, $B_{ij}=2\varepsilon_{ij}\left(R_{ij}^{*}\right)^{6}$ and $\varepsilon_{ij}=\left(\varepsilon_i\varepsilon_j\right)^{1/2}$

atoms	R*(Å)	ε_i (kcal.mol^{-1})
CT	1.9080	0.1094
C	1.9080	0.0860
OS	1.6837	0.170
O	1.6612	0.210
HC	1.4870	0.0157

W. D. Cornell et al., *J. Am. Chem. Soc.* **117**, 5179 (1997).

c) *pcff*: $\varepsilon_{ij}\left[2\left(\frac{r_{ij}^*}{r_{ij}}\right)^9-3\left(\frac{r_{ij}^*}{r_{ij}}\right)^6\right]$ with $\varepsilon_{ij}=2\left(\varepsilon_i\varepsilon_j\right)^{1/2}\frac{\left(r_i^*\right)^3\left(r_j^*\right)^3}{\left(r_i^*\right)^6+\left(r_j^*\right)^6}$ and $r_{ij}^*=\left(\frac{\left(r_i^*\right)^6+\left(r_j^*\right)^6}{2}\right)^{1/6}$

Atoms	r_i^* (Å)	ε_i (kcal.mol^{-1})
CT	4.010	0.054
C	3.810	0.120
OS	3.420	0.240
O	3.535	0.267
HC	2.995	0.020

Appendix 2

Partial charges for AMBER, and in bracket for *pcff* force fields.

atoms	q	Ref.	atoms	q	Ref.	atoms	q	Ref.
C_1	-0.120 (-0.106)	1	C_4	-0.180 (-0.159)	1	O_2	-0.430 (-0.531)	2
H_1C_1	0.066 (0.053)	1	H_1C_4	0.066 (0.053)	1	C_5	0.160 (0.066)	2
H_2C_1	0.066 (0.053)	1	H_2C_4	0.066 (0.053)	1	H_3C_5	0.030 (0.053)	2
C_2	0.000 (0.000)	1	H_3C_4	0.066 (0.053)	1	H_1C_5	0.030 (0.053)	2
C_3	0.510 (0.702)	2	O_1	-0.330 (-0.396)	2	H_2C_5	0.030 (0.053)	2

1) W. L. Jorgensen et al*., J. Am. Chem. Soc*., **118**, 11225(1996); 2) M. L. P. Price et al., *J. Comp. Chem.*, **22**, 1340 (2001)

Appendix 3

Parameters for bonding energetic term; a) for AMBER; b) for *pcff* force fields. For clarity, the mathematical expression is presented.

a) AMBER: $K\left(b-b_0\right)^2$

bonds	b_0 (Å)	k (kcal.mol^{-1}.Å^{-2})	Ref.
CT-CT	1.526	310.0	1
CT- C	1.522	317.0	1
CT-HC	1.090	340.0	2
CT-OS	1.410	320.0	1
C-O	1.229	570.0	1
C-OS	1.323	450.0	3

1) S.J. Weiner et al., *J. Comput. Chem.*, **7**, 230 (1986); 2) W. D. Cornell et al., *J. Am. Chem. Soc.* **117**, 5179 (1997); 3) J. Wang, et al., *J. Comput. Chem*., **21**, 1049 (2000).

b) *pcff*: $K_2\left(b-b_0\right)^2+K_3\left(b-b_0\right)^3+K_4\left(b-b_0\right)^4$

bonds	b_0 (Å)	k_2 (kcal.mol^{-1}.Å^{-2})	k_3 (kcal.mol^{-1}.Å^{-3})	k_4 (kcal.mol^{-1}.Å^{-4})
CT-CT	1.53	299.67	-501.77	679.81
CT-C	1.5202	253.7067	-423.037	396.9
CT-HC	1.1010	345.0	-691.89	844.6
CT-OS	1.43	326.7273	-608.5306	689.0333
C-O	1.202	851.1403	-1918.4882	2160.7659
C-OS	1.3683	367.1481	-794.7908	1055.2319

Appendix 4

Parameters for valence energetic term; a) for AMBER/OPLS; b) for *pcff* force fields.

a) AMBER: $H\left(\theta-\theta_0\right)^2$

angles	θ_0 (deg)	h (kcal.mol^{-1}.deg^{-2})	Ref.
CT-CT-CT	109.50	37.0	1
CT-CT-C	111.10	63.0	3
HC-CT-HC	109.50	28.5	3
CT-CT-HC	109.50	37.0	1
CT-C-O	120.40	80.0	2
CT-C-OS	115.00	80.0	2
O-C-OS	125.00	80.0	2
C-OS-CT	117.00	60.0	1

1) S.J. Weiner et al., *J. Comput. Chem.*, **7**, 230 (1986); 2) J. Wang, et al., *J. Comput. Chem.*, **21**, 1049 (2000); 3) J. Wang, et al., *J. Comput. Chem.*, **22**, 1219 (2000).

b) *pcff*: $H_2\left(\theta-\theta_0\right)^2+H_3\left(\theta-\theta_0\right)^3+H_4\left(\theta-\theta_0\right)^4$

angles	θ_0 (deg)	H_2 (kcal.mol^{-1}.deg^{-2})	H_3 (kcal.mol^{-1}.deg^{-3})	H_4 (kcal.mol^{-1}.deg^{-4})
CT-CT-CT	112.67	39.516	-7.443	-9.5583
CT-CT-C	108.53	51.9747	-9.4851	-10.9985
HC-CT-HC	107.66	39.641	-12.921	-2.4318
CT-CT-HC	110.77	41.453	-10.604	5.129
CT-C-O	123.145	55.5431	-17.2123	0.1348
CT-C-OS	100.318	38.8631	-3.8323	-7.9802
O-C-OS	120.797	95.3446	-32.2869	6.3778
C-OS-CT	113.288	61.2868	-28.9786	7.9929
OS-CT-HC	107.688	65.4801	-10.3498	5.8866

Appendix 5

Dihedral angle energetic term for AMBER, and in bracket for *pcff* force fields.

$$V_1\left[1-\cos\left(\phi-\phi_1^0\right)\right]+V_2\left[1-\cos\left(2\phi-\phi_2^0\right)\right]+V_3\left[1-\cos\left(3\phi-\phi_3^0\right)\right]$$

dihedral angles	V_1 (kcal.mol^{-1})	φ_1 (deg)	V_2 (kcal.mol^{-1})	φ_2 (deg)	V_3 (kcal.mol^{-1})	φ_3 (deg)	Ref.
CT-CT-CT-CT	0.22	180.0	0.34	180.0	0.195	0.0	4
	(0.00)	(0.0)	(0.0514)	(0.0)	(-0.1430)	(0.0)	
CT-CT-CT-C	0.00	0.0	0.00	0.0	0.1555	0.0	2
	(0.0972)	(0.0)	(0.0722)	(0.0)	(-0.2581)	()	
HC-CT-CT-CT	0.00	0.0	0.00	0.0	0.155	0.0	4
	(0.0000)	(0.0)	(0.0316)	(0.0)	(-0.1681)	(0.0)	
HC-CT-CT-HC	0.00	0.0	0.00	0.0	0.130	0.0	4
	(-0.1432)	(0.0)	(0.0617)	(0.0)	(-0.1083)	(0.0)	
CT-CT-C-O	0.00	0.0	0.00	0.0	0.067	180.0	1
	(0.0442)	(0.0)	(0.0292)	(0.0)	(0.0562)	(0.0)	
CT-CT-C-OS	0.00	0.0	0.00	0.0	0.000	0.0	1
	(1.8341)	(0.0)	(2.0603)	(0.0)	(-0.0195)	(0.0)	
CT-OS-C-CT	0.00	0.0	2.70	0.0	0.000	0.0	3
	(2.5594)	(0.0)	(2.2013)	(0.0)	(0.0325)	(0.0)	
O -C -OS-CT	1.40	180.0	2.70	180.0	0.000	0.0	4
	(0.0000)	(0.0)	(2.2089)	(0.0)	(0.0000)	(0.0)	
C-OS-CT-HC	0.00	0.0	0.00	0.0	0.3833	0.0	1
	(0.0000)	(0.0)	(0.0000)	(0.0)	(-0.1932)	(0.0)	

1) S.J. Weiner et al., *J. Comput. Chem.*, **7**, 230 (1986); 2) W. D. Cornell et al., *J. Am. Chem. Soc.* **117**, 5179 (1997); 3) J. Wang, et al., *J. Comput. Chem.*, **21**, 1049 (2000); 4) J. Wang, et al., *J. Comput. Chem.*, **22**, 1219 (2000).

5 REFERENCES

[1] D. Rigby, H. Sun and B. Eichinger, Computer simulations of poly(ethylene oxide): force field, pvt diagram and cyclization behaviour, *Polym. Int.* **1997**, *44*, 311.,

[2] N. L. Allinger, K. Chen and J. H. Lii, An improved force field (MM4) for saturated hydrocarbons, *J. Comput. Chem.* **1996**, *17*, 642.

[3] B. R. Gelin, *Molecular Modeling of Polymer Structures and Properties*, Hanser Publishers, Munich, 1994.

[4] U. M. Apel, R. Hentschke and J. Helfrich, Molecular dynamics simulation of syndio- and isotactic PMMA in benzene., *Macromolecules* **1995**, *28 (6)*, 1778-1785.

[5] A. Soldera, Comparison Between the Glass Transition Temperatures of the Two PMMA Tacticities: a Molecular Dynamics Simulation Point of View, *Macromol. Symp.* **1998**, *133*, 21-32

[6] A. Soldera, Energetic analysis of the two PMMA chain tacticities and PMA through molecular dynamics simulations, *Polymer* **2002**, *43*, 4269-4275.

[7] A. Soldera and Y. Grohens, Local Dynamics of Stereoregular PMMAs Using Molecule Simulation, *Macromolecules* **2002**, *35*, 722-726.

[8] A. Soldera and Y. Grohens, Cooperativity in stereoregular PMMAs observed by molecular simulation, *Polymer* **2004**, *45*, 1307-1311.

[9] M. Tsige and P. L. Taylor, Simulation study of the glass transition temperature in polymethylmethacrylate, *Phys. Rev. E.* **2002**, *65*, 021805.

[10] S. B. Sane, T. Cagin, W. G. Knauss and W. A. Goddard, Molecular dynamics simulations to compute the bulk response of amorphous PMMA, *J. Comput.Aided Mat. Des.* **2001**, *8*, 87-106.

[11] F. Jensen, *Introduction to Computational Chemistry*, John Wiley & Sons, Chichester, 1999.

[12] U. Burkert and N. L. Allinger, *Molecular Mechanics*, ACS, Washington, 1982.

[13] J. R. Maple, M.-J. Hwang, T. P. Stockfisch, U. Dinur, M. Waldman, C. S. Ewig and A. T. Hagler, Derivation of Class II force fields. 1. Methodology and quantum force field for the alkyl functional group and alkane molecules, *J. Comput. Chem.* **1994**, *15*, 162-182.

[14] E. Osawa and K. B. Lipkowitz. In: D. B. Boyd, D. B. Boyd. Reviews in Computational Chemistry, New York: VCH Publishers, Inc., 1995.

[15] D. A. Pearlman, D. A. Case, J. W. Caldwell, W. S. Ross, T. E. Cheatham III, S. DeBolt, D. Ferguson, G. Seibel and Kollman.P., AMBER, a package of computer programs for applying molecular mechanics, normal mode analysis, molecular dynamics and free energy calculations to simulate the structural and energetic properties of molecules, *Comp. Phys. Commun.* **1995**, *91*, 1-41.

[16] S. B. Sane, T. Cagin, W. G. Knauss and W. A. Goddard, Molecular dynamics simulations to compute the bulk response of amorphous PMMA, *J. Comput.Aided Mat. Des.* **2002**, *8*, 87-106.

[17] W. L. Jorgensen and J. Tiraod-Rives, *J. Am. Chem. Soc.* **1988**, *110*, 1657.

[18] M. P. Allen and D. J. Tildesley, *Computer Simulation of Liquids*, Clarendon Press, Oxford, 1987.

[19] H. Meirovitch, Computer simulation of self_avoiding walks: testing the scanning method, *J. Chem. Phys.* **1983**, *79(1)*, 502-508.

[20] D. N. Theodorou and U. W. Suter, Detailed molecular structure of a vinyl Polymer glass, *Macromolecules* **1985**, *18*, 1467-1478.

[21] M. Vacatello and P. J. Flory, Conformational Statistics of Poly(methyl methacrylate), *Macromolecules* **1986**, *19*, 405-415.

[22] W. Smith and T. R. Forrester, DL_POLY 2.14, *J. Molec. Graphics.* **1996**, *14*, 136.

[23] M. Parrinello and A. Rahman, *J. Appl. Phys.* **1981**, *52*, 7182.

[24] H. C. Andersen, MD simulations at constant pressure and/or temperature, *J. Chem. Phys.* **1980**, *72*, 2384.

[25] H. J. C. Berendsen, J. P. M. Postma, W. F. Van Gunsteren, DiNola, A. and J. R. Haak, Molecular dynamics with coupling to an external bath, *J. Chem. Phys.* **1984**, *81*, 3684-3690.

[26] D. Rigby and R. J. Roe, Molecular dynamics simulation of polymer liquid and glass. I. Glass transition., *J. Chem. Phys.* **1987**, *87(12)*, 7285-7292.

[27] R. H. Gee and R. H. Boyd, The role of the torsional potential in relaxation dynamics: a MD study of PE, *Comput. Theor. Polym. Sci.* **1998**, *8*, 91-98.

[28] C. F. Fan, T. Cagin, Shi W. and K. A. Smith, Local chain dynamics of a model polycarbonate near glass transition temperature: A MD simulation, *Macromol. Theory Simul.* **1997**, *6*, 83-102.

[29] J. Lub, F. C. B. M. Van Vroonhoven, D. Van Leyen and A. Benninghoven, *J. Polym. Sci., Part B: Polym. Phys.* **1989**, *27*, 2071.

[30] W. L. Jorgensen, D. S. Maxwell and J. Tirado-Rives, Development and Testing of the OPLS, *J. Am. Chem. Soc.* **1996**, *118*, 11225-11236

Biographies

Armand Soldera is assistant professor of molecular-physical chemistry at the Université de Sherbrooke, Québec, Canada. After obtaining a Ph.D. degree in the study of ferroelectric liquid crystals under the direction of Dr. D. Guillon and Pr. J.F. Nicoud, Université Louis Pasteur, Strasbourg, France, he undertook postdoctoral research with Pr. R.E. Prud'homme and Pr. C.G. Bazuin, Université Laval, Québec, Canada. Thereafter, he worked for eight years as research engineer in charge of the molecular modeling of polymers, at the Commissariat à l'Energie Atomique, CEA, France. He is also associated professor at the Institut Supérieur des Matériaux et Mécaniques Avancés, ISMANS, France. Since 2002, his studies are devoted to a perpetual interaction between experience and molecular modeling to better understand specific properties, and thus to enable the design of new compounds with optimal properties.

Nouteddine Metatla is a Ph.D. student under the supervision of Pr. A. Soldera at the Chemistry Department, Université de Sherbrooke, Québec, Canada. He presently works on the study of the difference in T_gs between stereoregular polymers by the use of molecular modeling of polymers. He received his B.Sc in Physics from the Annaba University, Algeria, and M.Sc. from the Nice Sophia Antipolis University, France.